JCTC Journal of Chemical Theory and Computation

Correcting Systematic Errors in DFT Spin-Splitting Energetics for Transition Metal Complexes

Thomas F. Hughes and Richard A. Friesner*

Columbia University, Department of Chemistry, New York, New York 10027, United States

Received June 28, 2010

Abstract: Spin-splittings of 57 octahedral first-row transition metal complexes calculated with B3LYP are compared with a database of experimental spectra collected from the literature. A variety of transition metal centers in various oxidation states and multiplicities along with a number of different coordinating ligands are considered. Environmental effects have been included to enable reasonable quantitative comparison with experiment. The manifold of states is studied using initial guesses constructed from ligand field theory. A localized orbital correction (LOC) model, referred to as DBLOC-DFT (d-block localized orbital corrected density functional theory), systematically corrects B3LYP calculations using five parameters. The final results are a considerable improvement over conventional DFT, bringing the mean unsigned error (MUE) from 10.14 kcal/mol with a standard deviation of 4.56 to 1.98 kcal/mol with a standard deviation of 1.62. Depending on the relative multiplicities of the ground and excited states, it is shown that B3LYP*, which has 15% exact nonlocal exchange, can lead to larger errors with respect to experiment than B3LYP. Application to 7 complexes from Swart et al. [*J. Phys. Chem. A* **2004**, *108*, 5479.] and 14 small-gap spin-crossover complexes, from the literature, shows the DBLOC model provides good agreement with a variety of experimental data.

1. Introduction

Transition metals play very important roles in biochemistry and materials science. The catalytic properties of metalloenzymes and other metal containing catalysts are a result of special electronic structures of reactive intermediates. As examples, consider the catalytic sites in methane monooxygenase[1] and the blue ruthenium dimer[2] for which the catalytically competent species have unusually large metal oxidation states along with important magnetic coupling interactions. The high density of low lying electronic states resulting from the metal atom can give rise to multiple reactive channels that can utilize spin-crossover[3−6] mechanisms. Here, otherwise high energy barriers become low energy through a facile change in spin multiplicity. Qualitatively, spin-crossover becomes possible when there is a balance between the pairing energy of two electrons and the ligand field splitting energy, Δ_o, needed to traverse the $t_{2g} \rightarrow e_g$ gap.[3] Splitting energies depend on metal−ligand interactions which range from weak interactions like simple electrostatically perturbed lone pairs to stronger dative bonds and finally more covalent bonds. In principle, these can be systematically tuned so as to control relative spin state energetics.

The energy difference between the t_{2g} and e_g sets of orbitals, Δ_o, has been found empirically to depend on the coordinating ligands according to the spectrochemical series[7−11]

$$I^{-1} < Br^{-1} < S^{-2} < NCS^{-1} < Cl^{-1} < NO_3^{-1} < N_3^{-1} < F^{-1} < OH^{-1} < C_2O_4^{-2} < H_2O < SCN^{-1} < CH_3CN < \text{pyridine} < NH_3 < \text{en} < \text{bipy} < \text{phen} < NO_2^{-1} < SO_3^{-2} < PPh_3 < CN^{-1} < CO$$

as well as the oxidation state of the metal center and the identity of the metal itself. Moving right in the series increases Δ_o, while decreasing the oxidation state of the metal decreases Δ_o so the balance of electronic effects becomes important. A large value of Δ_o signifies strong metal−ligand

* To whom correspondence should be addressed. E-mail: rich@chem.columbia.edu.

10.1021/ct100359x
Published on Web 12/07/2010

coupling, thereby raising the antibonding e_g orbital energies, oftentimes resulting in a low-spin ground state where the complex would rather pair electrons than spend additional energy in traversing the gap. Conversely, small values of Δ_o typically lead to high-spin complexes.

Requiring an electronic structure method to be capable of correctly predicting transition metal chemistry along with exhibiting calculation speed capable of handling large systems is a demanding request. It is well-known that the computation of a property like the spin-splitting energy is very sensitive to the quality of the underlying wave function. Two separate questions to answer are: what is the ground state multiplicity, and what is the energy for traversing the spin gap? Inclusion of factors like multireference character, dynamic correlation, spin−orbit coupling, relativity, vibronic coupling, as well as antiferromagnetic or ferromagnetic coupling for the case of transition metal clusters would be required for very high-level calculations. High-level methods, for example multireference many-body methods like coupled-cluster theory for transition metal systems, in principle offer a solution to the electronic problem, however, their computational cost, outside of massively parallel applications for which system size is still relatively small, renders it less useful in materials science and biology than density functional theory (DFT).[12−14]

Hybrid DFT methods such as B3LYP, the principal functional investigated in this work, provide an alternative to accurate, but computationally expensive, wave function-based approaches. Because even high-level approaches, such as coupled-cluster with perturbative triples (CCSD(T)), can be problematic for calculations involving transition metals,[15] DFT approaches, which for many cases deliver reasonable results, at present must be considered the method of choice for these systems. However, over the past decade, significant evidence has accumulated that even the best current DFT functionals can display large errors for specific types of transition metal energetics. As an example, different functionals can yield very different answers for spin state splittings by as much as 10−30 kcal/mol, and such errors can be manifested in comparisons with experimental data, for example in predicting the wrong ground state or in failure to properly yield small splittings in finely tuned spin-crossover complexes.

Despite the above observations, a detailed and comprehensive understanding of the performance of B3LYP, or any other functional, for spin state energetics is not currently available, in great part, because of the paucity and problematic nature of the available experimental data. Hence, as an initial step, we have constructed a chemically diverse database of solution and crystalline experimental spectra of 57 octahedral first-row transition metal containing complexes with different properties. Our database consists of 2 V,[16,17] 10 Cr,[7,17−23] 6 Mn,[23−26] 23 Ni,[22,27−34] 7 Fe,[35−39] and 9 Co[40−45] containing complexes with +2, +3, and +4 oxidation states, total charges ranging from −4 to +4, multiplicities ranging from 1 to 6, and total number of valence electrons ranging from 2 to 8. Coordinating atoms include C, N, O, S, F, and Cl with differing partial atomic charges, and the smallest and largest ligands contain 2 and 96 atoms, respectively. Ligands vary from mono- to hexa-dentate and in all cases are lone pair coordinated, i.e. metallocenes and other complexes with high hapticity are not considered here.

The variation in this database should be contrasted with alternative data sources such as electron paramagnetic resonance (EPR) or optical absorption measurements of spin-crossover complexes, where as has recently been pointed out by Deeth et al.,[46] the vast majority of complexes have aromatic nitrogens coordinated to Fe(II), and the ground states are uniformly low-spin singlets, with the excited state quintet requiring promotion of two electrons to a higher lying d-orbital, for example $t_{2g} \rightarrow e_g$. The spin-crossover data is useful but the drastic limitations noted above, the significance of which will become more apparent as we proceed with our analysis, has not been generally recognized.

To isolate the errors in the electronic problem from any potential errors because of the strong vibronic coupling effects and nonradiative transitions present at the spin-crossing seam, our database is based on equilibrium radiative spin-forbidden transitions under the Born−Oppenheimer approximation. Adiabatic potential energy surfaces are adequate because only regions that are far from the crossing are studied. These transitions are singly forbidden (the change in the number of unpaired electrons in going to the excited state is always two) d−d transitions that violate the spin selection rule and so they are of low intensity. Typically they show up in the optical absorption spectrum of the complex as shoulders to more intense spin allowed metal-to-ligand charge transfer (MLCT) or ligand-to-metal charge transfer (LMCT) transitions. Forbidden transitions become more intense by borrowing intensity from allowed transitions through spin−orbit coupling.

With a large, diverse database in hand, we observe large, but systematic, errors in the B3LYP computation of transition metal spin state splittings. However, these errors do not follow a pattern as simplistic as has been suggested in most DFT studies of these splittings to date.[47,48] While it is true that for the great majority of the aromatic nitrogen dominated spin-crossover complexes noted above (on which previous analysis has been primarily based), B3LYP shows an overstabilization of the high-spin state resulting in it being the ground state. But as is shown in detail below, other types of complexes can display very different behavior; for a substantial number of cases, we find in fact that low-spin states are very substantially overstabilized. A consequence of considering this much broader range of experimental systems is that solutions to the DFT spin-splitting problem proposed previously, such as decreasing the amount of exact nonlocal exchange in the hybrid functional, no longer yield even qualitatively satisfactory results. Nevertheless, striking regularities in the data are manifested, and a satisfactory model containing a modest number of parameters, all of which are physically based, can be constructed.

Most new DFT functional development has involved optimization of parameters internal to the DFT energy expression, as well as addition of new terms such as those involving the kinetic energy.[49,50] This approach has proved fruitful with new functionals such as the meta-GGA functional series of Truhlar and co-workers displaying substan-

tially improved prediction capabilities for a variety of properties.[50] A second approach, specific to transition metals, involves the adjustment of the amount of exact nonlocal exchange in hybrid functionals, for example the B3LYP* functional reduces the amount of exact nonlocal exchange in B3LYP from 20% to 15%.[48,51] This functional has been calibrated primarily with spin-crossover data, which, as discussed above, is apparently problematic.

Recently, we have introduced a simple, yet highly effective alternative to these approaches, in which localized, valence-bond-type empirical corrections are applied to specific chemical groups, fitting the parameter values to experimental data.[15,52−55] These corrections represent an improved estimation of nondynamical correlation effects in the targeted bonds and lone pairs, which are assumed to be transferable for well-defined localized chemical functionalities. Near-chemical accuracy has been achieved for molecules containing second and third-row atoms for thermodynamics, barrier heights, and electron affinities and ionization potentials, for large and diverse databases.[15,52−55] An initial paper extending this approach to transition metals was published several years ago[15] and yielded substantial improvements in energetics for atoms and small transition metal species, primarily a metal atom bonded to one small ligand. However, in that work we did not consider realistic organometallic complexes, such as those that comprise the present database.

In the present paper, we show that a suitably simple empirical correction scheme, entirely consistent with our previous work, and containing only five parameters which are readily physically interpretable, yields a dramatic reduction in the mean unsigned error (MUE) of the computed spin state gaps compared to experiment. The accuracy, MUE of around 2 kcal/mol, is consistent with that obtained in our previous transition metal work, and the MUE is somewhat higher than that for organic systems (MUE of around 1 kcal/mol) principally because of the lack of sufficient experimental data and the noise inherent in that data.

2. Methods

For many complexes we used published X-ray crystal structures for the initial geometries. In cases where these were not available we sometimes found a crystal structure for the complex with a different metal center or built the complex from crystal structures of multiligand complexes where only one ligand was of interest. The Cambridge Structural Database[56] was used. Especially for nickel-containing complexes, for reasons discussed below, it was sometimes necessary to use the minimized ground state geometry as opposed to the crystal structure as the initial structure for the excited state geometry minimizations.

All calculations were done using Jaguar version 7.5[57] with the relativistic effective core potential LACV3P, a triple-ζ contraction of the LACVP[58] basis set, for metal centers and 6-311G for the rest of the atoms. This basis set was chosen because it was successfully used in developing a localized orbital correction (LOC) model for transition metal atoms[15] and has been shown in the literature to work well in many standard DFT applications to metal containing systems. Previous work has shown that while the LOC corrections for metal atoms[15] do show some basis set dependence the differences in average error of the optimized model between the medium (LACV3P) and very large (QZVP(-g)) basis sets are small considering the great variety in the transition metal database.

Adiabatic spin state energy gaps are calculated using fully unrestricted pseudospectral B3LYP, with a continuum dielectric employed to model environmental effects. The Poisson−Boltzmann solver in Jaguar[57] was used. We used dielectric constant values for whatever solvent was used in obtaining the spectra experimentally, for example water has a value of 80.4, or in the case of crystalline spectra a low dielectric constant of 2.0 is used. Zero-point energy and entropic corrections were not determined because their difference with respect to states of different spin multiplicities are typically small.

The method of Langlois and co-workers[59] was used to generate initial guess density matrices, which take into account d−d electron repulsion and metal−ligand interactions. These guesses help to alleviate some of the difficulties that quantum chemical methods have with convergence to the ground states of the various multiplicities in transition metal containing systems. To ensure a more thorough search of state space we construct a series of initial guesses given a user specified table of atomic formal charges, localized multiplicities, and in the case of ferromagnetic or antiferromagnetic coupling, the number of coupled alpha- and beta-spins. In the case of magnetic coupling, broken symmetry DFT was used.[60] The default value of the relative energy threshold (keyword `opt325`) for acceptable initial guess electron configurations was changed from 0.1 hartree to 1.0 hartree to explore each of the different states generated by permuting single and paired electrons among the d-orbitals. Note that there were many times when the initial guess energy ordering of states, as well as obviously their relative magnitudes, was different from the converged UDFT values because of qualitative differences in the density matrices. Usually for calculations using the ground state multiplicity the lowest energy states are obtained using low values of the istate keyword, however, there were some exceptions. For calculations using the excited state multiplicities, this was certainly not true. Therefore the full range of `istate` values was considered in each case; this range can be precomputed using simple combinatorics

$$\texttt{istate} \in \left[1, \frac{5!}{s!d!(5-s-d)!}\right] \qquad (1)$$

where s and d are the number of singly and doubly occupied orbitals respectively in the set of five d-orbitals for the complex of a given multiplicity. The `istate` keyword simply specifies an initial guess for the electronic configuration of the metal complex in terms of singly and doubly occupied d-orbitals.

Adiabatic spin-forbidden transition energies are calculated using the lowest energy state of each spin multiplicity. To compare the calculated adiabatic transition energies with experimental vertical transitions the vibrational relaxation energies must be estimated. Franck−Condon factors could be calculated,[61] and the vibrational relaxation energy deter-

Table 1. Molecular Orbital Diagrams for Octahedral Metal Complexes with Spin-Forbidden Transitions

complex	type	num. val. elec.	g.s. mult.	g.s. l.f.d.	e.s. mult.	e.s. l.f.d.
cr223tetcl2, cracac2im2py, crccsime36, crcn6, crcyclamncs2, cren3, crf6, crnh34cl2, crnh36, crox3, mnf6	$t_{2g} \rightarrow t_{2g}$	3	4	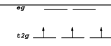	2	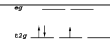
crf6, vf6, vurea6	$t_{2g} \rightarrow t_{2g}$	2	3	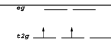	1	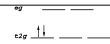
mn2p2pameth2, mncn6	$t_{2g} \rightarrow t_{2g}$	4	3	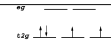	1	
ni12dimeim6, ni1meim6, ni2meim6, niacac2im2py, nibipy3, nibpm2no3, nidmso6, nidpdpm2h2o2, nidpdpm2no3h2o, nidpdpmno32, nidpdpmno32ch3cn, niedta, nien2scn2, nien3, nif6, nigly3, nih2o6, ninh36, niphen3, nipyrazole6, nitach3mepyr, nitpm2, nitpmno32	$e_g \rightarrow e_g$	8	3	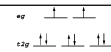	1	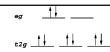
coamn3s3sarh, coamn5ssarh, coen3, coetn4s2amp, col2, con3s3, conh35soch32, conh36, fecn6	$t_{2g} \rightarrow e_g$	6	1	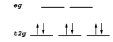	3	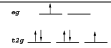
cof6	$e_g \rightarrow t_{2g}$	7	4		2	
fecn6, feen3	$t_{2g} \rightarrow e_g$	5	2	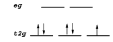	4	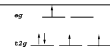
fecat3, feeta3, feh2o6, fethiocarbamate3, fetrencam, mnden2, mnen3, mnh2o6	$e_g \rightarrow t_{2g}$	5	6	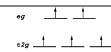	4	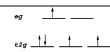

mined as a sum of vibrational energies up to the state with the most intense transition; however, we choose to take the difference between peak and onset values of the spin-forbidden shoulder from the experimental spectra so as to avoid, among other potential complications, having to calculate intensity contributions from the environment. Direct calculation of vertical transition energies is avoided because they would, at least in certain cases where the equilibrium geometries of the two states are significantly different, introduce additional errors inherent in nonequilibrium UDFT calculations. Additionally, some SCF convergence issues were found for vertical calculations. The protocol we have adopted enables a direct comparison between theory and experiment for the energy gaps between different spin states.

3. Results and Discussion

3.1. Database of $t_{2g} \rightarrow t_{2g}$, $e_g \rightarrow e_g$, $t_{2g} \rightarrow e_g$, and $e_g \rightarrow t_{2g}$ Spin-Forbidden Transitions for Octahedral Transition Metal Complexes. Table 1 shows the octahedral metal complexes in the DBLOC (d-block localized orbital corrected) database, including $t_{2g} \rightarrow t_{2g}$, $e_g \rightarrow e_g$, $t_{2g} \rightarrow e_g$, and $e_g \rightarrow t_{2g}$ ground to spin-forbidden excited state transitions. Table 1 of the Supporting Information shows models of the $t_{2g} \rightarrow t_{2g}$ complexes along with the names to which they will be referred (see Supporting Information Table 4 for a list of descriptors). There are a total of 16 complexes, 10 Cr(III), 1 Cr(IV), 2 Mn(III), 1 Mn(IV), and 2 V(III), of this type. From Table 1 note that crf6 is listed twice, once as $Cr(III)F_6^{-3}$ and once as $Cr(IV)F_6^{-2}$. The molecular orbital diagrams are shown in Table 1. These were determined using a combination of experimental results, ligand field theory, Mulliken spin densities and populations, and natural electron configurations.[62] A more detailed example of a molecular orbital diagram from hybrid DFT calculations on octahedral transition metal complexes was recently given by Watts et al.[63] It can be seen that energy differences between orbitals belonging to a given manifold, t_{2g} or e_g, are generally small. All complexes have high-spin ground states with the total number of valence d-electrons ranging from 2 to 4 with ground state multiplicities of 3 or 4 and excited state multiplicities of 1 or 2, respectively. In this work, the term "intermediate-spin" is not used because only two states are mainly considered, that is, one "low-spin" and one "high-spin. For example, a triplet might be referred to as "high-spin" relative to a "low-spin" singlet even though it is possible there could be an even higher spin state as in a quintet.

The same summary is provided for complexes with $e_g \rightarrow e_g$ spin-forbidden transitions in Table 1 (see Supporting Information Tables 2 and 5 for models of complexes and a

list of descriptors). In this case, there are 23 octahedral complexes all with d^8 Ni(II) centers. All transitions are from a high-spin triplet ground state to an excited state singlet.

Spin-forbidden transitions, $t_{2g} \rightarrow e_g$ or $e_g \rightarrow t_{2g}$, are considered at the bottom of Table 1 (see Supporting Information Tables 3 and 6 for models of complexes and a list of descriptors). There are 20 complexes including 1 Co(II), 8 Co(III), 1 Fe(II), 7 Fe(III), and 3 Mn(II). The various molecular orbital diagrams are shown in Table 1. In this case, all cobalt complexes have low-spin singlet ground states, with the exception of cof6 which has a quartet ground state. A pair of fecn6 complexes serve as examples of other low-spin ground state complexes, $Fe(III)(CN)_6^{-3}$ as a doublet ground state and $Fe(II)(CN)_6^{-4}$ as a singlet ground state. $Fe(III)(en)_3^{+3}$ has a doublet ground state. The rest of the complexes have a sextet ground state.

Minimized metal to coordinating atom bond distances are shown in Supporting Information Tables 7−9 for B3LYP/LACV3P minimizations in the appropriate environments for each of the spin states considered. During the minimizations, among a few other complexes, the excited state d^8 Ni(II) O_h complexes with coordinating nitrogens tended to drop to D_{4h} symmetry and become square planar when using B3LYP with a variety of basis sets. Most complexes are calculated to be slightly distorted octahedra where the metal−ligand bond distances are the degrees of freedom that undergo the largest change with a spin-forbidden transition. Bond distances are generally short in three particular cases (1) for states of lower multiplicity, (2) for complexes with a large number of valence electrons, and (3) for complexes with large metal oxidation states (see Supporting Information for a discussion).

3.2. Estimates of Vibrational Relaxation Energies. Estimates for the nonradiative vibrational relaxation energy for the $\nu_k \rightarrow \nu_0$ transition on the excited state surface are shown in Table 2. The difference in energy between the spin-forbidden highest intensity spectral peak ν_k and the lowest intensity spectral onset ν_0 is determined by using digitizing software.[64] Spin-forbidden shoulder peaks are extracted from higher intensity MLCT and/or LMCT peaks of the experimental spectra and fit to a dilated Lorentzian with two free parameters a and b

$$\mathcal{L}(x) = a\left(\frac{b}{(x - x_0)^2 + b^2}\right) \qquad (2)$$

where x_0 is the peak position. Relaxation energies for the experimental spectra of a number of different metal complexes with $t_{2g} \rightarrow t_{2g}$ and $e_g \rightarrow e_g$ spin-forbidden transitions were determined in this way. Using a unique vibrational relaxation energy for each complex was not possible, nor needed due to some inherent transferability in the electronic structure, because experimental spectra were not available in every case. Average peak to onset values of 1575 cm^{-1} (4.50 ± 1.41 kcal/mol) and 3206 cm^{-1} (9.17 ± 2.12 kcal/mol) were found. The results for cracac2im2py and niacac2im2py experiments, top and middle of Table 2, are representative examples of mean vibrational relaxation energies of $t_{2g} \rightarrow t_{2g}$ and $e_g \rightarrow e_g$ metal complexes and thus

Table 2. Estimate of the Nonradiative Relaxation Energy from the Highest (Spectral Peak, ν_k) to Lowest (Spectral Onset, ν_0) Intensity Vibrational States for the Excited Electronic State[a]

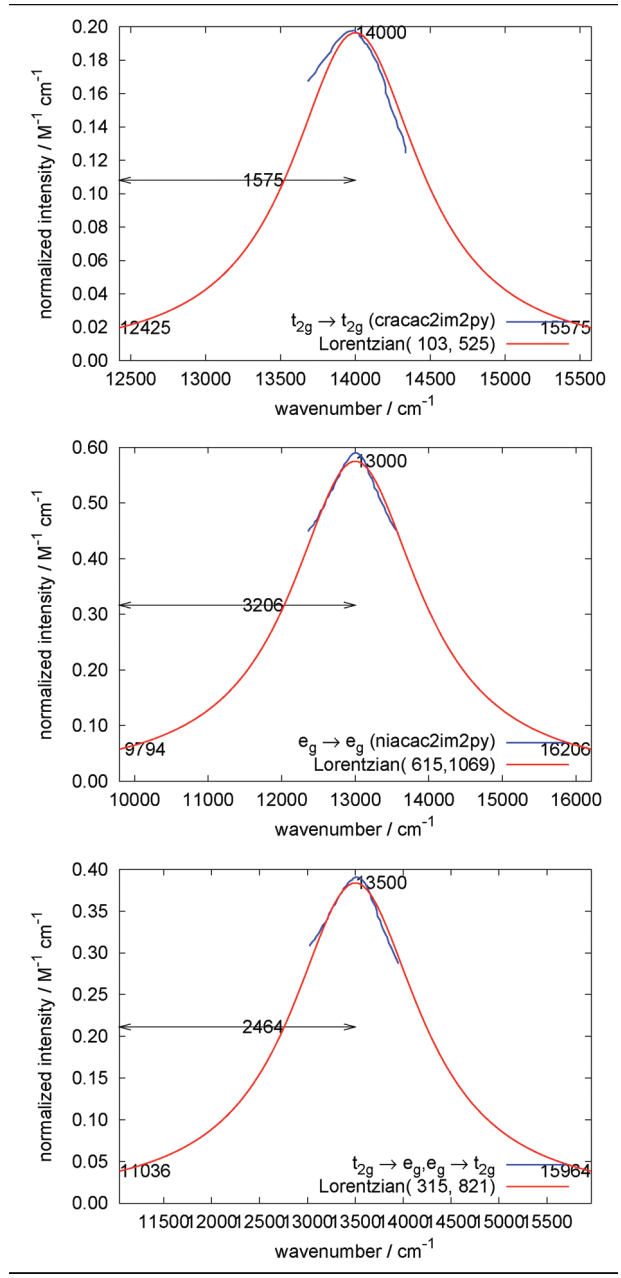

[a] Vibrational relaxation energies of 1575 ($t_{2g} \rightarrow t_{2g}$ top), 3206 ($e_g \rightarrow e_g$ middle), and 2464 cm^{-1} ($t_{2g} \rightarrow e_g$ or $e_g \rightarrow t_{2g}$ bottom) are obtained by subtracting the low intensity spectral onset (left) from the high intensity spectral peak. Spin-forbidden peaks, which typically show up as shoulder peaks to more intense MLCT or LMCT spin-conserving transitions, were resolved using digitizing software,[64] which extracts the coordinates from the experimental spectra shown in blue. These results were fit to a dilated Lorentzian, shown in red, with two free parameters.

are shown. More examples showing the fitted and experimental shoulder peaks for the $t_{2g} \rightarrow t_{2g}$ and $e_g \rightarrow e_g$ spin-forbidden transitions along with estimates for the vibrational relaxation energies are shown in Table 10 of the Supporting Information. For each of the types of transitions the estimates of the vibrational relaxation energies are within 1−2 kcal/

mol of each other. The vibrational relaxation energy for the $e_g \rightarrow e_g$ complexes is larger than that for the $t_{2g} \rightarrow t_{2g}$ complexes because the later transition involves an excitation within the nonbonding t_{2g} manifold, and so, there are less vibrational modes excited than for an excitation within the antibonding e_g manifold. This is in agreement with the observation that the change in the average calculated metal to ligand bond distances accompanying excitation are greater for the $e_g \rightarrow e_g$ complexes than for the $t_{2g} \rightarrow t_{2g}$ complexes. Subtracting these values from the experimentally determined peak spin-forbidden transition energies allows direct comparison with calculated adiabatic transitions.

An estimate of the vibrational relaxation energy for the spin-forbidden $t_{2g} \rightarrow e_g$ or $e_g \rightarrow t_{2g}$ transitions was determined using two different protocols. The first protocol involved fitting the shoulder peaks of the experiments for this class of complexes as was done for the $t_{2g} \rightarrow t_{2g}$ and $e_g \rightarrow e_g$ transitions (see Table 2 and Supporting Information Table 10 for examples). The second protocol was to fit the vibrational relaxation energies of the $t_{2g} \rightarrow t_{2g}$ (4.50 ± 1.41 kcal/mol) and $e_g \rightarrow e_g$ (9.17 ± 2.12 kcal/mol) transitions determined above with their adiabatic changes in bond distances and interpolate the vibrational relaxation energy for the $t_{2g} \rightarrow e_g$ or $e_g \rightarrow t_{2g}$ class of complexes. Using the average calculated metal−ligand bond distances, and one standard deviation to account for uncertainty, with values of 0.02 ($t_{2g} \rightarrow t_{2g}$), 0.15 ($e_g \rightarrow e_g$), and 0.12 Å ($t_{2g} \rightarrow e_g$ or $e_g \rightarrow t_{2g}$) (see the geometry section of the Supporting Information) an estimate for the vibrational relaxation energy was determined to be around 2800 cm^{-1} which is between the values determined for $t_{2g} \rightarrow t_{2g}$ and $e_g \rightarrow e_g$ transitions. The fitting of the shoulder peaks also predicts the relaxation energy to lie between the relaxation energies of the $t_{2g} \rightarrow t_{2g}$ and $e_g \rightarrow e_g$ transitions (see Supporting Information Table 10). Lastly an average of the $t_{2g} \rightarrow t_{2g}$ and $e_g \rightarrow e_g$ vibrational relaxation energies provides a further comparison. The difference in estimates between the protocols is small, about 1 kcal/mol, considering the approximate 2 kcal/mol MUE we are aiming at in this work. The final estimate for the vibrational relaxation energy of the $t_{2g} \rightarrow e_g$ or $e_g \rightarrow t_{2g}$ transitions is taken as 6.84 ± 1.68 kcal/mol. As previously mentioned this vibrational relaxation energy correction falls between the values determined for $t_{2g} \rightarrow t_{2g}$ and $e_g \rightarrow e_g$ transitions because here a single electron is moved to or from an antibonding e_g orbital as opposed to moving an electron within nonbonding t_{2g} or antibonding e_g and so the effective response of the e_g orbitals is intermediate. Further support for obtaining vibrational relaxation energies using this protocol is provided by noting that while the parameters of the DBLOC model were derived using vibrational relaxation corrected experimental gaps, those same DBLOC parameters provide very good results in comparison to experiments on near zero spin-crossover complexes for which the vibrational relaxation energy correction is zero.

3.3. $t_{2g} \rightarrow t_{2g}$ Energetics. A summary of experimental and calculated splittings in a dielectric continuum environment are shown in Tables 3 and 4 for the $t_{2g} \rightarrow t_{2g}$ spin-forbidden transitions. Experimental values, from which the 4.50 kcal/mol vibrational relaxation energy has been subtracted, range from 23.99 kcal/mol for vurea6 to 46.55 kcal/mol for mn2p2pameth2. With the exception of mn2p2pameth2 the experimental spin-forbidden transition energies cluster according to the molecular orbital diagrams at around 25 kcal/

Table 3. Experimental and Calculated Spin-Forbidden Transition Energies (kcal/mol) in a Dielectric Continuum Environment[a]

complex	mult.	$\langle S^2 \rangle$	exp.	B3LYP	B3LYP error
cr223tetcl2	2	0.83	36.53	49.14	−12.61
cr223tetcl2	4	3.78	0.00	0.00	0.00
crcn6	2	0.76	31.00	47.47	−16.47
crcn6	4	3.78	0.00	0.00	0.00
crcyclamncs2	2	0.79	34.54	49.51	−14.97
crcyclamncs2	4	3.78	0.00	0.00	0.00
cren3	2	0.78	38.67	54.09	−15.42
cren3	4	3.78	0.00	0.00	0.00
crf6	1	0.00	28.09	42.68	−14.59
crf6	3	2.02	0.00	0.00	0.00
crnh34cl2	2	1.03	36.95	51.80	−14.85
crnh34cl2	4	3.78	0.00	0.00	0.00
crnh36	2	0.78	39.15	55.50	−16.35
crnh36	4	3.77	0.00	0.00	0.00
crox3	2	0.86	36.53	48.83	−12.31
crox3	4	3.77	0.00	0.00	0.00
mncn6	1	0.00	24.10	35.45	−11.36
mncn6	3	2.03	0.00	0.00	0.00
mnf6	2	0.81	41.24	53.01	−11.77
mnf6	4	3.79	0.00	0.00	0.00

[a] For a pure spin ground state to a pure spin excited state, $t_{2g} \rightarrow t_{2g}$, the transition energy is larger than experiment.

Table 4. Experimental and Calculated Spin-Forbidden Transition Energies (kcal/mol) in a Dielectric Continuum Environment[a]

complex	mult.	$\langle S^2 \rangle$	exp.	B3LYP	B3LYP error
cr223tetcl2	2	1.75	36.53	25.17	11.36
cr223tetcl2	4	3.78	0.00	0.00	0.00
cracac2im2py	2	1.96	35.53	23.97	11.56
cracac2im2py	4	3.01	0.00	0.00	0.00
crccsime36	2	1.76	33.52	22.95	10.57
crccsime36	4	3.79	0.00	0.00	0.00
crcn6	2	1.76	31.00	23.54	7.46
crcn6	4	3.78	0.00	0.00	0.00
crcyclamncs2	2	1.76	34.54	24.78	9.76
crcyclamncs2	4	3.78	0.00	0.00	0.00
cren3	2	1.75	38.67	27.04	11.63
cren3	4	3.78	0.00	0.00	0.00
crf6	2	1.75	40.37	25.89	14.48
crf6	4	3.76	0.00	0.00	0.00
crf6	1	1.00	28.09	13.13	14.96
crf6	3	2.02	0.00	0.00	0.00
crnh34cl2	2	1.75	36.95	26.08	10.87
crnh34cl2	4	3.78	0.00	0.00	0.00
crnh36	2	1.75	39.15	26.78	12.36
crnh36	4	3.77	0.00	0.00	0.00
crox3	2	1.75	36.53	24.58	11.95
crox3	4	3.77	0.00	0.00	0.00
mn2p2pameth2	1	0.00	46.55	39.94	6.62
mn2p2pameth2	3	2.02	0.00	0.00	0.00
mncn6	1	1.01	24.10	12.54	11.56
mncn6	3	2.03	0.00	0.00	0.00
mnf6	2	1.76	41.24	26.74	14.50
mnf6	4	3.79	0.00	0.00	0.00
vf6	1	1.00	24.66	12.53	12.13
vf6	3	2.00	0.00	0.00	0.00
vurea6	1	1.00	23.99	13.31	10.68
vurea6	3	2.01	0.00	0.00	0.00

[a] For a pure spin ground state to a contaminated spin excited state, $t_{2g} \rightarrow t_{2g}$, the transition energy is smaller than experiment.

mol for $Cr(IV)F_6^{-2}$, mncn6, vf6, and vurea6, and at around 37 kcal/mol for the rest of the complexes. The DFT results cluster similarly. Note that the set of complexes that cluster around 25 kcal/mol are those that are ground state triplets, as opposed to ground state quartets like the other complexes, and so the lower spin-forbidden transition energy is attributed to a smaller spin−spin stabilization energy as can be seen in the molecular orbital diagrams in Table 1. In both tables, B3LYP predicts the correct ordering of ground and excited state multiplicities in every case. The effects of the environment were found to be significant for some of the highly charged complexes and in aligning the states, that is, reducing the standard deviation in the errors. Preliminary vacuum results for the chromium series, confining ourselves at the time to only the first couple of istate values, showed wildly, seemingly random, differing results for the spin-forbidden transition energies, by as much as 12 kcal/mol. With the use of solvent they were later found to correspond to different electronic states.

Table 3 shows that the B3LYP/LACV3P predicts one excited state to lie above the experiment by about 14 kcal/mol while in Table 4 it predicts a different excited state to lie below the experiment by about 11 kcal/mol. These are the two low-lying states present in the excited state manifold. Given that spin-forbidden transitions have zero dipole oscillator strength, some means of calculating the spin-forbidden transition intensity, Franck−Condon intensities[61] and potentially spin−orbit coupling terms[65] would be necessary to definitively tell which state corresponds to the correct mapping onto the shoulders observed in the experimental spectrum. Comparing Tables 3 and 4 shows that the high-energy state is a more restrictive spin pure state, while the low energy state is spin contaminated with the high-spin ground state. All ground states are pure spin with the exception of cracac2im2py. Three key facts suggest that the lower of the two spin states obtained from our B3LYP calculation is in fact the state corresponding to the shoulder seen in the optical absorption spectrum. First, as noted above, this state has ground state multiplicity mixed into the wave function, which facilitates the borrowing of intensity as compared to the higher energy state, which has no such admixture. Second, the higher energy state is not present in a significant number of our B3LYP computations, whereas the lower state is always present. This could be the result of failure to employ a suitable initial guess, but it also may be the case that the state is mixed with other excited states or has moved to a substantially higher energy. Third, the shoulder is the lowest-energy feature in the experimental optical absorption spectrum, and asserting its correspondence with the lowest-energy computed DFT state makes sense. Additionally, similar reasoning is used in a recent article by Watts et al.[63] where hybrid DFT methods are able to reproduce the experimental observation that temperature dependent magnetic moments of some iron-porphyrin complexes clearly show high-spin states for some ligands and a mix of high and intermediate spin states for others thereby resulting in a calculated pure spin state for the former and a mixed spin state for the later. On the basis of these arguments, we shall assume the stated correspondence in the analysis that follows. The achievement of consistency and accuracy in the numerical results for the energetics, if attained, will provide further evidence that this fundamental assumption that we are making is in fact correct.

Grouping the metal complexes in Table 1 according to molecular orbital diagrams and comparing to Table 4 shows that the average error for t_{2g}^2, t_{2g}^3, and t_{2g}^4 configurations is 12.59 kcal/mol, 11.50 kcal/mol, and 9.09 kcal/mol. B3LYP/LACV3P clearly has a large intrinsic error in the pairing of two t_{2g} electrons and smaller errors for the spin−spin interactions. A preliminary systematic correction scheme in which t_{2g}^2 and t_{2g}^4 are treated as identical cases predicts a pairing correction of around 10 kcal/mol. The most striking characteristic of the data in Table 4 is that the errors, compared to experiment, are tightly grouped around the value of 10 kcal/mol, and hence a single empirical parameter of this magnitude can drastically reduce the error for complexes of the type $t_{2g} \rightarrow t_{2g}$. We interpret this value as the B3LYP/LACV3P error that is manifested when a d-electron in an organometallic complex is moved from a singly occupied t_{2g} orbital to another singly occupied t_{2g} orbital to form a doubly occupied t_{2g} orbital. The sign of the correction implies that the low-spin form is overstabilized with respect to experiment. This is consistent with our previous work.[15,52] There, we observed that specific types of orbitals can manifest overbinding, due to overestimation of nondynamical correlation effects. The d-orbitals have a different shape and size, and further interact with ligands, hence the errors seen here are different from those in a bare metal atom.[15] We employ the same value, around 10 kcal/mol, of this correction for all metals in the $t_{2g} \rightarrow t_{2g}$ database and for all oxidation states. Whether the identical value can be used for the e_g manifold is addressed in the next section. In our final empirical model, there are also corrections due to differing numbers of spin−spin interactions in the ground and excited states; this correction is relatively small, and is discussed further below when we present the final model which is optimized by least-squares fitting to all of the experimental data simultaneously.

3.4. $e_g \rightarrow e_g$ Energetics. Energies for the $e_g \rightarrow e_g$ spin-forbidden transitions of the Ni(II) complexes are shown in Table 5. Experimental triplet to singlet transitions, which have been reduced by 9.17 kcal/mol for the vibrational relaxation energy, range from 23.14 kcal/mol for nitach3mepyr to 33.72 kcal/mol for nif6. Table 5 shows the lower-energy spin-contaminated excited state, which has similar spin expectation values and errors in the energies as those values from Table 4. This is as expected because in both cases the molecular orbital diagrams in Table 1 show that the differences in the electronic structures between ground and excited states are simply the pairing of two electrons. The average error for the spin-forbidden transition energies is around 10 kcal/mol, a value consistent with the $t_{2g} \rightarrow t_{2g}$ transitions. This consistency validates both the protocol for analyzing the experimental data and the theoretical model explaining the origin of the DFT error in splittings for cases in which there is transfer of an electron within the t_{2g} or e_g manifolds, as opposed to between manifolds.

Table 5. Experimental and Calculated Spin-Forbidden Transition Energies, $e_g \rightarrow e_g$, (kcal/mol) in a Dielectric Continuum Environment

complex	mult.	$\langle S^2 \rangle$	exp.	B3LYP	B3LYP error
ni12dimeim6	1	1.00	29.09	18.27	10.82
ni12dimeim6	3	2.00	0.00	0.00	0.00
ni1meim6	1	1.00	28.43	16.94	11.48
ni1meim6	3	2.00	0.00	0.00	0.00
ni2meim6	1	1.00	28.47	18.10	10.37
ni2meim6	3	2.00	0.00	0.00	0.00
niacac2im2py	1	1.77	28.00	18.14	9.86
niacac2im2py	3	3.78	0.00	0.00	0.00
nibipy3	1	0.00	25.11	13.07	12.04
nibipy3	3	2.00	0.00	0.00	0.00
nibpm2no3	1	0.92	27.64	15.76	11.88
nibpm2no3	3	2.00	0.00	0.00	0.00
nidmso6	1	1.00	30.94	17.46	13.48
nidmso6	3	2.01	0.00	0.00	0.00
nidpdpm2h2o2	1	1.00	28.95	17.66	11.29
nidpdpm2h2o2	3	2.00	0.00	0.00	0.00
nidpdpm2no3h2o	1	0.99	28.95	17.22	11.74
nidpdpm2no3h2o	3	2.00	0.00	0.00	0.00
nidpdpmno32	1	0.10	28.95	14.02	14.94
nidpdpmno32	3	2.00	0.00	0.00	0.00
nidpdpmno32ch3cn	1	0.89	28.95	17.22	11.73
nidpdpmno32ch3cn	3	2.00	0.00	0.00	0.00
niedta	1	1.00	27.00	16.84	10.16
niedta	3	2.00	0.00	0.00	0.00
nien2scn2	1	0.97	27.03	15.11	11.92
nien2scn2	3	2.00	0.00	0.00	0.00
nien3	1	0.71	26.08	8.09	17.99
nien3	3	2.00	0.00	0.00	0.00
nif6	1	1.00	33.72	19.41	14.31
nif6	3	2.00	0.00	0.00	0.00
nigly3	1	1.00	28.29	17.42	10.87
nigly3	3	2.00	0.00	0.00	0.00
nih2o6	1	0.91	33.03	18.99	14.04
nih2o6	3	2.00	0.00	0.00	0.00
ninh36	1	1.00	28.23	17.35	10.87
ninh36	3	2.00	0.00	0.00	0.00
niphen3	1	0.10	25.16	7.84	17.32
niphen3	3	2.00	0.00	0.00	0.00
nipyrazole6	1	1.00	28.86	17.52	11.34
nipyrazole6	3	2.00	0.00	0.00	0.00
nitach3mepyr	1	1.00	23.14	16.64	6.51
nitach3mepyr	3	2.01	0.00	0.00	0.00
nitpm2	1	1.00	27.78	17.54	10.24
nitpm2	3	2.01	0.00	0.00	0.00
nitpmno32	1	0.91	27.58	17.87	9.71
nitpmno32	3	2.00	0.00	0.00	0.00

Table 6. Experimental and Calculated Spin-Forbidden Transition Energies, $t_{2g} \rightarrow e_g$ or $e_g \rightarrow t_{2g}$, (kcal/mol), in a Dielectric Continuum Environment

complex	mult.	$\langle S^2 \rangle$	exp.	B3LYP	B3LYP error
coamn3s3sarh	1	0.00	0.00	0.00	0.00
coamn3s3sarh	3	2.21	33.61	21.99	11.62
coamn5ssarh	1	0.00	0.00	0.00	0.00
coamn5ssarh	3	2.11	32.48	24.09	8.38
coen3	1	0.00	0.00	0.00	0.00
coen3	3	2.04	32.33	29.32	3.01
coetn4s2amp	1	0.00	0.00	0.00	0.00
coetn4s2amp	3	2.13	32.62	25.27	7.35
cof6	2	1.75	43.20	31.76	11.44
cof6	4	3.75	0.00	0.00	0.00
col2	1	0.00	0.00	0.00	0.00
col2	3	2.04	23.74	21.97	1.77
con3s3	1	0.00	0.00	0.00	0.00
con3s3	3	2.18	34.72	22.36	12.36
conh35soch32	1	0.00	0.00	0.00	0.00
conh35soch32	3	2.04	26.22	23.42	2.80
conh36	1	0.00	0.00	0.00	0.00
conh36	3	2.04	30.33	29.79	0.55
fecat3	4	3.79	22.61	22.59	0.02
fecat3	6	8.76	0.00	0.00	0.00
fecn6	1	0.00	0.00	0.00	0.00
fecn6	3	2.04	60.93	37.40	23.52
fecn6	2	0.76	0.00	0.00	0.00
fecn6	4	3.80	45.14	28.58	16.57
feen3	2	0.79	0.00	0.00	0.00
feen3	4	3.81	18.89	20.91	−2.02
feeta3	4	3.79	25.19	21.87	3.32
feeta3	6	8.76	0.00	0.00	0.00
feh2o6	4	3.77	29.19	23.84	5.35
feh2o6	6	8.76	0.00	0.00	0.00
fethiocarbamate3	4	3.99	11.75	6.57	5.18
fethiocarbamate3	6	8.76	0.00	0.00	0.00
fetrencam	4	3.80	22.90	24.21	−1.31
fetrencam	6	8.76	0.00	0.00	0.00
mnden2	4	3.77	39.05	28.64	10.42
mnden2	6	8.75	0.00	0.00	0.00
mnen3	4	3.77	38.05	27.71	10.34
mnen3	6	8.75	0.00	0.00	0.00
mnh2o6	4	3.76	47.12	43.44	3.67
mnh2o6	6	8.75	0.00	0.00	0.00

3.5. $t_{2g} \rightarrow e_g$ and $e_g \rightarrow t_{2g}$ Energetics. There is much greater variation in the electronic structures shown in Table 1 for the last set of spin-forbidden transitions because there are both excitations, $t_{2g} \rightarrow e_g$, and de-excitations, $e_g \rightarrow t_{2g}$, on going from a ground state of one multiplicity to an excited state of another multiplicity. The $t_{2g} \rightarrow e_g$ and $e_g \rightarrow t_{2g}$ database has the largest variation in experimental results with transition energies ranging from 11.75 kcal/mol for fethiocarbamate3 to 60.93 kcal/mol for Fe(II)$(CN)_6^{-4}$. Please see the Supporting Information discussion section for more details about the experimental results. Here all of the cobalt complexes, with the exception of cof6, along with the two fecn6 complexes (Fe(II)$(CN)_6^{-4}$ and Fe(III)$(CN)_6^{-3}$) and the feen3 complex, have low-spin ground states while the rest of the complexes have high-spin ground states like the $t_{2g} \rightarrow t_{2g}$ and $e_g \rightarrow e_g$ complexes. Any set of empirical corrections to the B3LYP results must be robust enough to ensure both consistency and accuracy across this database, a task which may be challenging considering the substantial variation observed in the B3LYP error in Table 6. Emphasis is on comparing the B3LYP with the experimental spin-forbidden transition energies keeping in mind the ligand field splitting parameter, Δ_o, that empirically depends on ligands according to the spectrochemical series as well as on metal oxidation state.

While an electron changes manifolds, $t_{2g} \rightarrow e_g$ or $e_g \rightarrow t_{2g}$, the cases being considered here still involve interconversion between two singly occupied orbitals and one doubly occupied orbital, although the singly occupied orbitals are now in two different manifolds. Thus, the pairing correction described previously will still be enforced, as will the spin−spin interaction correction. However, a major new possible source of error has been introduced, which is the DFT calculation of the splitting between the t_{2g} and e_g manifolds. From the data in Table 6, it is clear that this error must be significant, as the error pattern across the various complexes is quite different from the uniformity seen in the previous two classes of complexes, exhibiting substantial variation in magnitude.

A review of the basic physics of the origin of the splitting provides a useful starting point for understanding how the DFT error is likely to depend upon the chemical nature of the transition metal complex. The t_{2g} orbitals have minimal interaction with the ligand lone pairs that are pointed at the metal, and are to a first approximation viewed as nonbonding orbitals. The e_g orbitals in contrast can have a strong interaction with the ligand orbitals. The importance of this interaction depends primarily upon two factors: the energy of the relevant ligand orbitals, and overlap of these orbitals with the e_g metal d-orbitals. Qualitatively, higher energies of the ligand orbitals (bringing them closer in energy to the metal d-orbitals) and greater overlap of ligand and metal d-orbitals leads to a larger mixing of the ligand and e_g orbitals, and this in turn is reflected in an increase in the energy of the e_g orbitals which essentially take on the role of low lying antibonding orbitals of the complex. The ligand orbitals that interact with the e_g orbitals in turn play the role of bonding orbitals, and are pushed downward in energy by greater mixing. When the $t_{2g} \rightarrow e_g$ splitting is large compared to the pairing energy of two d-electrons, the t_{2g} orbitals are filled prior to any occupation of the e_g orbitals, leading to a low-spin complex in the ground state. In contrast, when the splitting is small compared to the pairing energy, the e_g orbitals are singly occupied prior to double occupation of any t_{2g} orbitals, and a high-spin state becomes the ground state.

DFT based errors in the Δ_o splitting must be dominated by errors in the matrix elements between the ligand and metal d-orbitals that interact to form the new e_g orbitals. The metal−ligand "bonding" characterizing such interactions can be viewed as having a large ionic character. There is a strong dependence of these nondynamical correlation errors on DFT functional, which explains why different functionals yield very different prediction of relative transition metal spin state energetics. For B3LYP, in an ionic complex such as NaCl, the strength of the ionic bond (which in turn is proportional to the Hamiltonian matrix element between the appropriate Na^+ and Cl^- orbitals) is underestimated by 4.5 kcal/mol.[52] Such an underestimation will in turn lead to an equivalent underestimation of the splitting of the t_{2g} and e_g orbitals, and this underestimation will stabilize high-spin, as opposed to low-spin, states. This is the origin of the observation in the literature concerning the apparent overstabilization of high-spin complexes by B3LYP and other hybrid functionals.

We expect each ligand lone pair coordinated to the metal to contribute a component to the error. The magnitude of the contribution should be on the same energy scale as the bond energy errors seen for organic systems, roughly 1−5 kcal/mol. Finally, the value of the error will depend predominantly upon the ligand and, secondarily, upon the metal and oxidation state, and we expect to see a semiquantitative correlation with the spectrochemical series. The most accurate model would be derived by assigning a large number of parameters for different ligands depending upon their chemical structure, however, we lack sufficient data to do this in a fine grained fashion. Hence, to avoid overfitting, we instead try to use the smallest number of ligand parameters possible in the analysis that follows. This leads to a "minimalist" model which nevertheless displays remarkable predictive power. Future versions of the model aimed at higher accuracy will likely need to increase the number of ligand parameters as is briefly discussed below.

By grouping the complexes in Table 1 according to their molecular orbital diagrams, as well as coordinating atoms and metal oxidation states, it can be seen that the experimental results cluster accordingly and are consistent considering the spectrochemical series and spin−spin stabilization energies. Again it is seen that a balance in the electronic structure becomes important for example consider the similarity in the spin-splitting energies for complexes with differing electronic structures as in Co complexes with $t_{2g} \rightarrow e_g$ versus Fe complexes with $e_g \rightarrow t_{2g}$, as well as balancing the effect of decreasing Δ_o with an oxidation state less than two with increasing Δ_o with strongly interacting ligands as in $Fe(II)(CN)_6^{-4}$. In every case the correct ordering of the states is obtained with B3LYP and in many cases the conventional B3LYP was already close to experiment.

Each Co(III)-N6 complex, coen3, col2, conh35soch32, and conh36 involves an unpairing of a t_{2g} orbital worth around −10 kcal/mol. This is the same pairing error as determined before for the $t_{2g} \rightarrow t_{2g}$ and $e_g \rightarrow e_g$ complexes but with opposite sign. By comparing the −10 kcal/mol with the average error in the spin-forbidden transition energy, which is already reasonably small, around 2 kcal/mol, a Δ_o correction is determined to be around 2 kcal/mol per coordinating nitrogen. As will be discussed below all values will be optimized by linear regression for the final DBLOC model. Proceeding similarly for the Co(III) nitrogen and sulfur complexes, coamn3s3sarh, coamn5ssarh, coetn4s2amp, and con3s3, there is an unpairing correction of −10 kcal/mol along with the 2 kcal/mol per nitrogen for the $t_{2g} \rightarrow e_g$ excitation. Comparison to the experimental gap provides a larger Δ_o correction of 5 kcal/mol per sulfur atom. Note that with the exception of the small outlier coamn5ssarh the error increases as the number of coordinating thio-ether sulfurs increases.

For higher multiplicity calculations the singly occupied−singly occupied (t_{2g} or e_g) interaction becomes important and depending on the oxidation state and ligands very small Δ_o can induce some interaction between t_{2g} and e_g electrons. Considering fethiocarbamate3 there are corrections of 10 kcal/mol for pairing and a total of −12 kcal/mol for de-exciting in a field of six anionic sulfurs. The later comes from the fact that anionic sulfurs lie to the left of the spectrochemical series and thus receive a 2 kcal/mol correction per atom. Comparing the sum with the error in the spin-forbidden transition of 5 kcal/mol gives an estimate for creating a singly occupied−singly occupied interaction at around −1 kcal/mol. The fethiocarbamate3 despite being a +3 oxidation state complex loses 7 such interactions because anionic sulfurs are so far left in the spectrochemical series thereby inducing spin−spin stabilization between the t_{2g} and e_g manifolds. The Fe(III)−O6 complexes having a small average error can be analyzed using the same types of corrections as for fethiocarbamate3, except that in this case,

Table 7. Final Five DBLOC Correction Parameters for Spin-Forbidden Transitions Optimized by Linear Regression[a]

symbol	description	value (kcal/mol)
p	create a doubly occupied orbital	10.05/pair
ss	create a singly occupied−singly occupied interaction	−1.05/interaction
exlss	$t_{2g} \rightarrow e_g$ excitation (left spectrochemical series)	1.88/atom
exmss	$t_{2g} \rightarrow e_g$ excitation (middle spectrochemical series)	2.85/atom
exrss	$t_{2g} \rightarrow e_g$ excitation (right spectrochemical series)	5.21/atom

[a] The values shown are for the pairing of electrons, the creation of a spin−spin interaction, or for $t_{2g} \rightarrow e_g$ excitation for the excited state relative to the ground state. Note that the last three parameters are corrections for Δ_o.

we only lose 3 spin−spin interactions and the de-excitation is in a field of six oxygens. This includes both neutral oxygen, as in the aquo ligand, and anionic oxygen, as in the hydroxyl ligand. These ligands are again to the left of the spectrochemical series and so the same parameters are used giving reasonable results. For the Mn(II)−N6 and Mn(II)−O6 complexes, there are pairing and de-excitation parameters along with the loss of 7 spin−spin interactions because of the +2 oxidation state. Co(II)-F6 has a total correction of around 11 kcal/mol which is composed only of the pairing correction and the loss of 3 spin−spin corrections. This is because the oxidation state is +2 and the fluoride ion lies far to the left of the spectrochemical series. This complex has roughly 5-fold degenerate d-orbitals and is more comparable to the $t_{2g} \rightarrow t_{2g}$ or $e_g \rightarrow e_g$ class of complexes. Since the cyano ligand is to the far right of the spectrochemical series it is more comparable to the 5 kcal/mol correction for the thio-ether sulfur containing ligands, and so Fe(II)−C6, along with the pairing correction, results in a total correction of 20 kcal/mol. Analyzing the Fe(III)−C6 complex proceeds similarly except for the formation of a spin−spin interaction.

3.6. DBLOC Model. A simplified correction scheme can now be devised for calculating accurate relative spin state energetics of transition metal complexes. An acceptable ratio of parameters to data points has been achieved. The final set of five DBLOC parameters optimized by linear regression are shown in Table 7 and the errors with respect to experiment of the corrected spin-forbidden transition energies are shown in Table 8. The parameter exmss will be discussed in the section below on small-gap spin-crossover complexes but is included now for completeness. The DBLOC energy, E_{DBLOC}, is given by adding the DBLOC correction, $E_{\mathrm{DBLOC}}^{\mathrm{corr}}$, to the B3LYP energy, E_{B3LYP},

$$E_{\mathrm{DBLOC}} = E_{\mathrm{B3LYP}} + E_{\mathrm{DBLOC}}^{\mathrm{corr}} \quad (3)$$

where

Table 8. Errors (kcal/mol) with Respect to Experiment for the DBLOC Corrected Spin-Forbidden Transition Energies, along with the Weights of the Parameters Shown in Table 7[a]

complex	p	ss	exlss	exmss	exrss	exp.	B3LYP error	DBLOC error
cr223tetcl2	1	−3	0	0	0	36.53	11.36	−1.82
cracac2im2py	1	−3	0	0	0	35.53	11.56	−1.63
crccsime36	1	−3	0	0	0	33.52	10.57	−2.61
crcn6	1	−3	0	0	0	31.00	7.46	−5.73
crcyclamncs2	1	−3	0	0	0	34.54	9.76	−3.43
cren3	1	−3	0	0	0	38.67	11.63	−1.56
crf6	1	−3	0	0	0	40.37	14.48	1.30
crf6	1	−1	0	0	0	28.09	14.96	3.87
crnh34cl2	1	−3	0	0	0	36.95	10.87	−2.31
crnh36	1	−3	0	0	0	39.15	12.36	−0.82
crox3	1	−3	0	0	0	36.53	11.95	−1.24
mn2p2pameth2	1	−1	0	0	0	46.55	6.62	−4.47
mncn6	1	−1	0	0	0	24.10	11.56	0.47
mnf6	1	−3	0	0	0	41.24	14.50	1.31
vf6	1	−1	0	0	0	24.66	12.13	1.04
vurea6	1	−1	0	0	0	23.99	10.68	−0.41
ni12dimeim6	1	−1	0	0	0	29.09	10.82	−0.27
ni1meim6	1	−1	0	0	0	28.43	11.48	0.39
ni2meim6	1	−1	0	0	0	28.47	10.37	−0.72
niacac2im2py	1	−1	0	0	0	28.00	9.86	−1.23
nibipy3	1	−1	0	0	0	25.11	12.04	0.95
nibpm2no3	1	−1	0	0	0	27.64	11.88	0.79
nidmso6	1	−1	0	0	0	30.94	13.48	2.39
nidpdpm2h2o2	1	−1	0	0	0	28.95	11.29	0.20
nidpdpm2no3h2o	1	−1	0	0	0	28.95	11.74	0.64
nidpdpmno32	1	−1	0	0	0	28.95	14.94	3.84
nidpdpmno32ch3cn	1	−1	0	0	0	28.95	11.73	0.64
niedta	1	−1	0	0	0	27.00	10.16	−0.93
nien2scn2	1	−1	0	0	0	27.03	11.92	0.83
nien3	1	−1	0	0	0	26.08	17.99	6.89
nif6	1	−1	0	0	0	33.72	14.31	3.21
nigly3	1	−1	0	0	0	28.29	10.87	−0.22
nih2o6	1	−1	0	0	0	33.03	14.04	2.95
ninh36	1	−1	0	0	0	28.23	10.87	−0.22
niphen3	1	−1	0	0	0	25.16	17.32	6.23
nipyrazole6	1	−1	0	0	0	28.86	11.34	0.25
nitach3mepyr	1	−1	0	0	0	23.14	6.51	−4.59
nitpm2	1	−1	0	0	0	27.78	10.24	−0.85
nitpmno32	1	−1	0	0	0	27.58	9.71	−1.38
coamn3s3sarh	−1	0	3	0	3	33.61	11.62	0.42
coamn5ssarh	−1	0	5	0	1	32.48	8.38	3.85
coen3	−1	0	6	0	0	32.33	3.01	1.81
coetn4s2amp	−1	0	4	0	2	32.62	7.35	−0.52
cof6	1	−3	0	0	0	43.20	11.44	−1.75
col2	−1	0	6	0	0	23.74	1.77	0.56
con3s3	−1	0	3	0	3	34.72	12.36	1.16
conh35soch32	−1	0	6	0	0	26.22	2.80	1.59
conh36	−1	0	6	0	0	30.33	0.55	−0.66
fecat3	1	−3	−6	0	0	22.61	0.02	−1.91
fecn6	−1	0	0	0	6	60.93	23.52	2.33
fecn6	−1	1	0	0	6	45.14	16.57	−3.58
feen3	−1	1	6	0	0	18.89	−2.02	−2.18
feeta3	1	−3	−6	0	0	25.19	3.32	1.38
feh2o6	1	−3	−6	0	0	29.19	5.35	3.42
fethiocarbamate3	1	−7	−6	0	0	11.75	5.18	−0.94
fetrencam	1	−3	−6	0	0	22.90	−1.31	−3.24
mnden2	1	−7	−6	0	0	39.05	10.42	4.30
mnen3	1	−7	−6	0	0	38.05	10.34	4.22
mnh2o6	1	−7	−6	0	0	47.12	3.67	−2.45

[a] The $t_{2g} \rightarrow t_{2g}$, $e_g \rightarrow e_g$, and $t_{2g} \rightarrow e_g$ or $e_g \rightarrow t_{2g}$ are at the top, middle, and bottom, respectively.

$$E_{\mathrm{DBLOC}}^{\mathrm{corr}} = \frac{1}{2}({}^{0}n_{\alpha}^{t_{2g}} - {}^{k}n_{\alpha}^{t_{2g}} + {}^{0}n_{\alpha}^{e_g} - {}^{k}n_{\alpha}^{e_g})p + \lambda({}^{k}n_{\alpha}^{t_{2g}}{}^{k}n_{\alpha}^{e_g} - {}^{0}n_{\alpha}^{t_{2g}}{}^{0}n_{\alpha}^{e_g})\mathrm{ss} + \frac{1}{2}({}^{k}n_{\alpha}^{t_{2g}}({}^{k}n_{\alpha}^{t_{2g}} - 1) + {}^{k}n_{\alpha}^{e_g}({}^{k}n_{\alpha}^{e_g} - 1) - {}^{0}n_{\alpha}^{t_{2g}}({}^{0}n_{\alpha}^{t_{2g}} - 1) - {}^{0}n_{\alpha}^{e_g}({}^{0}n_{\alpha}^{e_g} - 1))\mathrm{ss} + ({}^{0}n^{t_{2g}} - {}^{k}n^{t_{2g}}) \times \sum_{i=1}^{6}(\mathrm{exlss}\delta_{L_i 0} + \mathrm{exmss}\delta_{L_i 1} + \mathrm{exrss}\delta_{L_i 2}) \quad (4)$$

$$\lambda \approx H(2 - q)H(3 - (L_1 + L_2 + L_3 + L_4 + L_5 + L_6)) \quad (5)$$

with ${}^{0}n_{\alpha}^{t_{2g}}$, ${}^{k}n_{\alpha}^{t_{2g}}$, ${}^{0}n_{\alpha}^{e_g}$, and ${}^{k}n_{\alpha}^{e_g}$ being the number of unpaired t_{2g} or e_g electrons for the ground, 0th, and excited states,

kth, respectively. The total number of t_{2g} electrons for the ground and excited states are given by ${}^{0}n^{t_{2g}}$ and ${}^{k}n^{t_{2g}}$. The parameter λ turns on spin−spin interactions between the t_{2g} and e_g manifolds for the case of small Δ_o, that is, where the Heaviside functions, $H(2 - q)$ or $H(3 - (L_1 + L_2 + L_3 + L_4 + L_5 + L_6))$, become positive in cases where the metal has oxidation state less than or equal to 2 or when the sum of ligand integers (discussed below) is less than or equal to around 3. The sum is over the first coordination sphere of an octahedral complex where the value of L_i indicates wether the coordinating atom lies to the left ($L_i = 0$), middle ($L_i = 1$), or right ($L_i = 2$) of the spectrochemical series and the Kronecker delta selects the appropriate term. Parameters p, ss, exlss, exmss, and exrss are the DBLOC model parameters. Sign conventions for the parameters are as shown for either creating an electron pair (p), creating a spin−spin interaction (ss), or for moving an electron from $t_{2g} \rightarrow e_g$ (exlss, exmss, and exrss, depending upon the ligand atoms coordinated to the metal) as the complex transitions from the ground to the excited state. Note that the parameter ss is applied per interaction, while the parameters exlss, exmss, and exrss are applied per coordinating atom. Opposite signed parameters must be used if the ground to excited state transition involves the opposite of the listed physical process. This reversibility of the parameters with reversibility of the physical interpretation provides support for the robustness of the underlying model. For example, the pairing parameter at 10.05 kcal/mol changes sign if unpairing electrons. The magnitude of this value signifies the importance of errors in B3LYP's description of nondynamical correlation of occupied d-orbitals in metal complexes. The $t_{2g} \rightarrow e_g$ excitation parameters, exrss, exmss, and exlss, are different because the error in the B3LYP depends on the position of the coordinating atoms in the spectrochemical series. For this database the error increases from 1.88 to 2.85 and finally to 5.21 kcal/mol as we move to the right of the spectrochemical series corresponding to a larger Δ_o and thus more strongly interacting ligands. As noted above, the signs and magnitudes of these corrections, when interpreted in a simple ligand field picture, are in remarkably good correspondence with the analogous range of correction parameters analyzed for metal atoms[15] and organic molecules.[52]

In general, B3LYP largely underestimates the energy required to pair two t_{2g} or e_g electrons, overestimates the energy to unpair them, slightly overestimates the energy of a parallel spin−spin interaction, and underestimates the size of Δ_o, more severely for strongly interacting ligands. Table 8 shows that the MUE for conventional B3LYP goes from 11.40 kcal/mol (standard deviation of 2.25 kcal/mol) to 2.13 kcal/mol (standard deviation of 1.53 kcal/mol) for $t_{2g} \rightarrow t_{2g}$, from 11.95 kcal/mol (standard deviation of 2.51 kcal/mol) to 1.77 kcal/mol (standard deviation of 1.96 kcal/mol) for $e_g \rightarrow e_g$, and from 7.05 kcal/mol (standard deviation of 6.06 kcal/mol) to 2.11 kcal/mol (standard deviation of 1.27 kcal/mol) for $t_{2g} \rightarrow e_g$ or $e_g \rightarrow t_{2g}$. This is an overall decrease from 10.14 kcal/mol (standard deviation of 4.56 kcal/mol and maximum of 23.52 kcal/mol) to 1.98 kcal/mol (standard deviation of 1.62 kcal/mol and maximum of 6.89 kcal/mol). This maximum error is for nien3 which is one of the complexes for which B3LYP/LACV3P has some difficulties in breaking the octahedral symmetry. To summarize, the DBLOC model performs extremely well energetically and removes many outliers. Complexes crcn6, mn2p2pameth2, nitach3mepyr, and feh2o6 show only minor improvement while the error for some complexes increases only slightly.

Table 9. Comparison of Errors for Conventional B3LYP (20% Exact Non-Local Exchange), B3LYP* (15% Exact Non-Local Exchange), and DBLOC with Experimental Spin-Forbidden Transition Energies (kcal/mol) for Selected Complexes, crnh36 ($t_{2g} \rightarrow t_{2g}$), nigly3 ($e_g \rightarrow e_g$), cof6 and fetrencam ($e_g \rightarrow t_{2g}$), and fecn6 ($t_{2g} \rightarrow e_g$)[a]

complex	mult.	exp.	B3LYP error	B3LYP* error	error diff.	DBLOC error
crnh36	2	39.15	12.36	15.06	2.70	−0.83
crnh36	4	0.00	0.00	0.00	0.00	0.00
nigly3	1	28.29	10.85	16.15	5.31	−0.24
nigly3	3	0.00	0.00	0.00	0.00	0.00
cof6	2	43.20	11.45	19.75	8.30	−1.74
cof6	4	0.00	0.00	0.00	0.00	0.00
fecn6	2	0.00	0.00	0.00	0.00	0.00
fecn6	4	45.14	16.59	12.82	−3.77	−3.56
fetrencam	4	22.90	−1.32	0.52	1.84	−3.25
fetrencam	6	0.00	0.00	0.00	0.00	0.00

[a] For all complexes but fecn6, the ground state is high-spin. B3LYP's stabilization of the high-spin states relative to B3LYP* results in better agreement with experiment in all cases except fecn6. The DBLOC model shows considerable improvement over both B3LYP and B3LYP*. The column error diff is the difference between B3LYP* and B3LYP errors.

Application of the DBLOC model to 7 metal complexes studied by Swart et al.[66] (see Supporting Information Tables 11−13) shows systematic results for similar chemical species and illustrates that although it is possible for the model to reorder the spin states, the correct ordering of the states given by conventional DFT is preserved by DBLOC. The spin multiplicities of the ground states of these complexes are known, however, the experimental gaps remain unknown.

3.7. Comparison to B3LYP*. Comparison of errors for conventional B3LYP, B3LYP* (5% less exact nonlocal exchange than B3LYP), and DBLOC single point LACV3P calculations with experiment for some selected complexes are shown in Table 9. The complexes are crnh36, which is $t_{2g} \rightarrow t_{2g}$, nigly3, which is $e_g \rightarrow e_g$, cof6 and fetrencam, which are $e_g \rightarrow t_{2g}$, and fecn6, which is $t_{2g} \rightarrow e_g$, and experimentally all are high-spin ground states with the exception of fecn6. The results shown for B3LYP and DBLOC and their comparison with experiment are the same as the results previously discussed. As expected, comparing the B3LYP* and B3LYP total energies (not shown) shows that reducing the amount of exact nonlocal exchange makes the energies less negative. The important differences, shown in the relative energies, are that the high-spin states undergo a larger change than the low-spin states resulting in smaller spin gaps for complexes with high-spin ground states and larger spin gaps for complexes with low-spin ground states. For these experimental spin-forbidden transitions reducing the amount of exact nonlocal exchange brings the final B3LYP* result further from experiment by about 5 kcal/mol on average in every case except fecn6 for which the results are closer to experiment by about 4 kcal/mol. Similar problems would be manifested in many other complexes in our database. In

Table 10. Molecular Orbital Diagrams for the Octahedral Small-Gap Spin-Crossover Complexes Studied in Refs 47, 48, and 67

complex	type	num. val. elec.	g.s. mult.	g.s. l.f.d.	e.s. mult.	e.s. l.f.d.
feacac2trien	$t_{2g} \rightarrow e_g$	5	2	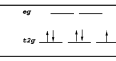	6	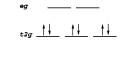
fepapth2, fetacn2, fe2amp3, fehbpz32, fepybzimh3, fetppn3, fephen2ncs2, fetpen, fetpancs2, febptnncs2, fephen2ncse2	$t_{2g} \rightarrow e_g$	6	1		5	
coterpy2, copyimine22	$t_{2g} \rightarrow e_g$	7	2	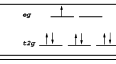	4	

Table 11. Application of DBLOC to Spin-Crossover Complexes with Near-Zero Spin Gap[a]

complex	p	ss	exlss	exmss	exrss	exp.	B3LYP	B3LYP error	DBLOC	DBLOC error
feacac2trien	−2	4	8	4	0	2.87	−3.11	5.98	−0.97	3.84
fepapth2	−2	2	0	12	0	3.82	−8.13	11.95	3.87	−0.05
fetacn2	−2	2	12	0	0	5.50	−5.02	10.52	−4.66	10.16
fe2amp3	−2	2	6	6	0	5.26	−7.17	12.43	−0.99	6.25
fehbpz32	−2	2	0	12	0	4.54	−0.72	5.26	11.28	−6.74
fepybzimh3	−2	2	0	12	0	5.02	−6.93	11.95	5.07	−0.05
fetppn3	−2	2	4	8	0	6.69	−5.26	11.95	2.86	3.83
coterpy2	−1	1	0	6	0	3.11	−4.78	7.89	1.22	1.89
copyimine22	−1	1	0	6	0	3.35	−6.21	9.56	−0.21	3.56
fephen2ncs2	−2	2	4	8	0	0.00	−7.98	7.98	0.14	−0.14
fetpen	−2	2	4	8	0	0.00	−2.29	2.29	5.83	−5.83
fetpancs2	−2	2	6	6	0	0.00	−3.99	3.99	2.19	−2.19
febptnncs2	−2	2	8	4	0	0.00	−8.22	8.22	−3.98	3.98
fephen2ncse2	−2	2	4	8	0	0.00	−7.43	7.43	0.69	−0.69

[a] B3LYP and experimental results are taken from the literature. The first nine complexes are from ref 47, while the last four are from ref 67. Results for fephen2ncs2 are taken from ref 48. The majority of the complexes are ground state singlet Fe(II)−N6 (most with aromatic nitrogens) crossing over to a high-spin quintet thereby changing the number of unpaired electrons by four.

contrast, DBLOC provides systematically appropriate corrections, in sign and magnitude, across the entire suite of test cases. The reason for the failure of B3LYP* for these test cases is straightforward. When applied to the "standard" set of spin-crossover complexes, the B3LYP errors are generally in the 5−10 kcal/mol range and the high-spin state is overstabilized due to reduction of Δ_o as discussed previously. The presence of a $e_g \rightarrow t_{2g}$ transition between the ground and relevant excited spin states, and the numerical value of the error in the energy gap, are a consequence of the metals in these compounds being primarily Fe or Co and the ligands virtually all being aromatic nitrogens, as noted above. These are the cases for which B3LYP* was optimized, and subsequent "tests" of the method employed cases that differ very little in the aforementioned key respects. The test cases we have presented, in which B3LYP* performs poorly, in contrast involve different metals and ligands, and in many cases involve movement of the electron exclusively in the t_{2g} or e_g manifold. The overfitting of B3LYP* to a narrowly defined training set then becomes apparent, and its unsuitability for general use manifest.

3.8. Applications to Small-Gap Spin-Crossover Complexes. Molecular orbital diagrams of a number of small-gap spin-crossover octahedral complexes from the literature are shown in Table 10 (see Supporting Information Table 14 for models of complexes). The first 9 complexes are from ref 47, the fephen2ncs2 complex is from ref 48. and the last 4 complexes are from ref 67. Some of the complexes from the last reference have not been included here because the DFT results reported show heavy dependence on both functional and basis set and there are not enough calculation details provided to resolve this. Most of the complexes are low-spin singlet ground state Fe(II)−N6 (and most of the N atoms are aromatic) involving a spin-crossover to the high-spin quintet, where there are 4 more unpaired electrons. All of these complexes have either one or two $t_{2g} \rightarrow e_g$ nonradiative transitions.

Table 11 shows B3LYP and experimental spin-crossover energetics for the small-gap complexes. The B3LYP results reported here are simply those values reported in the literature and vibrational relaxation effects do not need to be taken into account given the experimental protocols used in these cases. Details of the B3LYP calculations and the experimental results are described in the literature.[47,48,67] In every case conventional B3LYP incorrectly reverses the ordering of the spin states with respect to experiment, predicting the high-spin state to be the ground state by as much as 8 kcal/mol. This is in agreement with the observation that B3LYP tends to overbind high-spin states and hence these are the ground states for complexes with near zero gaps. Experimental gaps are all within about 5 kcal/mol. On average the conventional B3LYP spin-crossover energies have errors

with respect to experiment of 8.39 kcal/mol with a standard deviation of 3.21 kcal/mol and a maximum error of 12.43 kcal/mol.

Using the literature B3LYP and experimental results shown in Table 11 for the spin-crossover energy shows the DBLOC models necessity of the exmss parameter of 2.85 kcal/mol for aromatic nitrogen in correcting the small-gap spin-crossover data. DBLOC corrects the B3LYP ordering of the spin states in all but 2 important cases (fetacn2 and febptnncs2). The MUE for DBLOC is 3.51 kcal/mol with a standard deviation of 2.98 kcal/mol and a maximum of 10.16 kcal/mol. This MUE and maximum error might be substantially decreased if we were to recompute the B3LYP DFT results using our standard basis sets and convergence protocol, an analysis we plan to carry out in the near future. As it is, the reduction of MUE from 8.39 to 3.51 kcal/mol, with no further adjustment of parameters and no recomputation of DFT with a single consistent basis set, represents a very substantial improvement.

4. Conclusion

A simplified five-parameter empirical correction scheme based on ligand field theory is proposed to give more accurate energies for B3LYP calculations on relative spin state energetics of transition metal complexes. By isolating errors in radiative spin-forbidden transition energies over a diverse database of octahedral transition metal complexes some general rules about the behavior of B3LYP in comparison to experiment can be made. Errors in the treatment of nondynamical correlation of occupied d-orbitals results in B3LYP's large underestimation, 10.05 kcal/mol, of the energy required to pair two t_{2g} or e_g electrons. Additionally, errors in Δ_o were found to be proportional to the strength of the metal−ligand interaction, that is, smaller, 1.88 kcal/mol, intermediate, 2.85 kcal/mol, and larger, 5.21 kcal/mol, corrections to the left, middle, and right of the spectrochemical series. B3LYP also slightly overestimates parallel spin−spin interactions in metal complexes. The DBLOC model brings the average error in the spin-splitting from 10.14 to 1.98 kcal/mol. Comparison of B3LYP, B3LYP*, and DBLOC clearly shows the advantages of using DBLOC over B3LYP and B3LYP* (15% exact nonlocal exchange) for which the spin-forbidden transition errors are often worse than B3LYP by about 5 kcal/mol. Applying DBLOC to the seven complexes from Swart et al.[66] shows that it is in agreement with experiment. Applying DBLOC to spin-crossover compounds with near zero gaps reduces the MUE of conventional B3LYP from 8.39 to 3.51 kcal/mol.

Acknowledgment. This work has been supported by the Department of Energy program through solar photochemistry (DE-FG02-90ER-14162) to R.A.F.

Supporting Information Available: Tables of B3LYP equilibrium geometries for the various DBLOC metal complexes in their different spin states, along with discussion of these results, experimental results for $t_{2g} \rightarrow e_g$ and $e_g \rightarrow t_{2g}$ spin-forbidden transitions, tables and discussion describing the application of the DBLOC model to complexes from Swart et al.,[66] additional tables including models of complexes, DBLOC database descriptors, and supplementary vibrational relaxation data, and Cartesian coordinates of all complexes. This material is available free of charge via the Internet at http://pubs.acs.org.

References

(1) Rinaldo, D.; Philipp, D.; Lippard, S.; Friesner, R. *J. Am. Chem. Soc.* **2007**, *129*, 3135.

(2) Concepcion, J.; Jurss, J.; Brennaman, M.; Hoertz, P.; Patrocinio, A.; Iha, N.; Templeton, J.; Meyer, T. *Acc. Chem. Res.* **2009**, *42*, 1954.

(3) Gutlich, P.; Hauser, A.; Spiering, H. *Angew. Chem., Int. Ed. Engl.* **1994**, *33*, 2024.

(4) Harvey, J. N.; Aschi, M. *Faraday Discuss.* **2003**, *124*, 129.

(5) Carreón-Macedo, J.-L.; Harvey, J. N. *Phys. Chem. Chem. Phys.* **2006**, *8*, 93.

(6) Conradie, J.; Ghosh, A. *J. Phys. Chem. B* **2007**, *111*, 12621.

(7) Ballhausen, C. J. *Introduction to Ligand Field Theory*; McGraw-Hill Book Company, Inc.: New York, 1962.

(8) Douglas, B.; McDaniel, D.; Alexander, J. *Concepts and Models of Inorganic Chemistry*; John Wiley & Sons Inc.: New York, 1994.

(9) Steinfeld, J. I. *Molecules and Radiation: An Introduction to Modern Molecular Spectroscopy*; The MIT Press, Inc.: Cambridge, MA, 1985.

(10) Harris, D. C.; Bertolucci, M. D. *Symmetry and Spectroscopy: An Introduction to Vibrational and Electronic Spectroscopy*; Oxford University Press, Inc.: New York, 1978.

(11) Shimura, Y. *Bull. Chem. Soc. Jpn.* **1988**, *61*, 693.

(12) Friesner, R.; Guallar, V. *Annu. Rev. Phys. Chem.* **2005**, *56*, 389.

(13) Siegbahn, P. E. M.; Borowski, T. *Acc. Chem. Res.* **2006**, *39*, 729.

(14) Cramer, C.; Truhlar, D. *Phys. Chem. Chem. Phys.* **2009**, *11*, 10757.

(15) Rinaldo, D.; Tian, L.; Harvey, J.; Friesner, R. A. *J. Chem. Phys.* **2008**, *129*, 164108.

(16) Nolet, M.-C.; Beaulac, R.; Boulanger, A.-M.; Reber, C. *Struct. Bonding* **2004**, *107*, 145.

(17) Allen, G. C.; El-Sharkawy, G. A. M. *Inorg. Nucl. Chem. Lett.* **1970**, *6*, 493.

(18) Vanquickenborne, L. G.; Coussens, B.; Postelmans, D.; Ceulemans, A.; Pierloot, K. *Inorg. Chem.* **1991**, *30*, 2978.

(19) Friesen, D. A.; Nashiem, R. E.; Waltz, W. L. *Inorg. Chem.* **2007**, *46*, 7982.

(20) Choi, J.-H.; Choi, S. Y.; Hong, Y. P.; Ko, S.-O.; Ryoo, K. S.; Lee, S. H.; Park, Y. C. *Spectrochim. Acta, Part A* **2008**, *70*, 619.

(21) Berben, L. A.; Long, J. R. *Inorg. Chem.* **2005**, *44*, 8459.

(22) Tsukahara, Y.; Kamatani, T.; Lino, A.; Suzuki, T.; Kaizaki, S. *Inorg. Chem.* **2002**, *41*, 4363.

(23) Stewart J. J. P. Mopac. http://openmopac.net/manual/Transition_metal_complexes.html, 2010.

(24) Jørgensen, C. K. *Inorg. Chim. Acta* **1969**, *3*, 313.

(25) Arulsamy, N.; Hodgson, D. J. *Inorg. Chem.* **1994**, *33*, 4531.

(26) Manson, N. B.; Shah, G. A.; Howes, B.; Flint, C. D. *Mol. Phys.* **1977**, *34*, 1157.

(27) Childers, M. L.; Su, F.; Przyborowska, A. M.; Bishwokarma, B.; Park, G.; Brechbiel, M. W.; Torti, S. V.; Torti, F. M.; Broker, G.; Alexander, J. S.; Rogers, R. D.; Ruhlandt-Senge, K.; Planalp, R. P. *Eur. J. Inorg. Chem.* **2005**, *19*, 3971.

(28) Baho, N.; Zargarian, D. *Inorg. Chem.* **2007**, *46*, 299.

(29) Nolet, M.-C.; Michaud, A.; Bain, C.; Zargarian, D.; Reber, C. *Photochem. Photobiol.* **2006**, *82*, 57.

(30) González, E.; Rodrigue-Witchel, A.; Reber, C. *Coord. Chem. Rev.* **2007**, *251*, 351.

(31) Buñuel, M. A.; García, J.; Proietti, M. G.; Solera, J. A.; Cases, R. *J. Chem. Phys.* **1999**, *110*, 3566.

(32) Bussiére, G.; Reber, C.; Neuhauser, D.; Walter, D. A.; Zink, J. I. *J. Phys. Chem. A* **2003**, *107*, 1258.

(33) Reimann, C. W. *J. Phys. Chem.* **1970**, *74*, 561.

(34) Jørgensen, C. K. *Acta Chem. Scand.* **1955**, *9*, 1362.

(35) Ewald, A. H.; Martin, R. L.; Ross, I. G.; White, A. H. *Proc. Royal Soc. A* **1964**, *280*, 235.

(36) Renovitch, G. A.; Baker, W. A. *J. Am. Chem. Soc.* **1968**, *90*, 3585.

(37) Naiman, C. S. *J. Chem. Phys.* **1961**, *35*, 323.

(38) Gray, H. B.; Beach, N. A. *J. Am. Chem. Soc.* **1963**, *85*, 2922.

(39) Karpishin, T. B.; Gebhard, M. S.; Solomon, E. I.; Raymond, K. N. *J. Am. Chem. Soc.* **1991**, *113*, 2977.

(40) Maiti, D.; Paul, H.; Chanda, N.; Chakraborty, S.; Mondal, B.; Puranik, V. G.; Lahiri, G. K. *Polyhedron* **2004**, *23*, 831.

(41) Sharrad, C. A.; Lüthi, S. R.; Gahan, L. R. *Dalt. Trans.* **2003**, *19*, 3693.

(42) Goodall, D. M.; Hollis, D. B.; White, M. S. *J. Phys. Chem.* **1987**, *91*, 4255.

(43) Bruce, J. I.; Gahan, L. R.; Hambley, T. W.; Stranger, R. *Inorg. Chem.* **1993**, *32*, 5997.

(44) Donlevy, T. M.; Gahan, L. R.; Hambley, T. W.; McMahon, K. L.; Stranger, R. *Aust. J. Chem.* **1993**, *46*, 1799.

(45) J. Ferguson, D. L. W.; Knox, K. *J. Chem. Phys.* **1963**, *39*, 881.

(46) Deeth, R. J.; Anastasi, A. E.; Wilcockson, M. J. *J. Am. Chem. Soc.* **2010**, *132*, 6876.

(47) Jensen, K. P.; Cirera, J. *J. Phys. Chem. A* **2009**, *113*, 10033.

(48) Reiher, M. *Inorg. Chem.* **2002**, *41*, 6928.

(49) Zhao, Y.; Truhlar, D. G *J. Chem. Phys.* **2006**, *125*, 194101.

(50) Zhao, Y.; Truhlar, D. G. *Theor. Chem. Acc.* **2008**, *120*, 215.

(51) Salomon, O.; Reiher, M.; Artur Hess, B. *J. Chem. Phys.* **2002**, *117*, 4729.

(52) Friesner, R. A.; Knoll, E. H.; Cao, Y. *J. Chem. Phys.* **2006**, *125*, 124107.

(53) Knoll, E. H.; Friesner, R. A. *J. Phys. Chem. B* **2006**, *110*, 18787.

(54) Goldfeld, D.; Bochevarov, A.; Friesner, R. A. *J. Chem. Phys.* **2008**, *129*, 214105.

(55) Hall, M.; Goldfeld, D.; Bochevarov, A.; Friesner, R. A. *J. Chem. Theory Comput.* **2009**, *5*, 2996.

(56) Allen, F. H. *Acta Crystallogr.* **2002**, *B58*, 380.

(57) *Jaguar*, version 7.5; Schrödinger, Inc.: New York, NY, 2009.

(58) Hay, P. J.; Wadt, W. R. *J. Chem. Phys.* **1985**, *82*, 299.

(59) Vacek, G.; Perry, J. K.; Langlois, J.-M. *Chem. Phys. Lett.* **1999**, *310*, 189.

(60) Noodleman, L. *J. Chem. Phys.* **1981**, *74*, 5737.

(61) Berger, R.; Fischer, C.; Klessinger, M. *J. Phys. Chem. A* **1998**, *102*, 7157.

(62) Reed, A.; Weinstock, R.; Weinhold, F. *J. Chem. Phys.* **1985**, *83*, 735.

(63) Liao, M.-S.; Huang, M.-J.; Watts, J. D. *J. Phys. Chem. A* **2010**, *114*, 9554.

(64) Engauge Digitizer, http://digitizer.sourceforge.net, 2010.

(65) Berning, A.; Schweizer, M.; Werner, H.-J.; Knowles, P. J.; Palmieri, P. *Mol. Phys.* **2000**, *98*, 1823.

(66) Swart, M.; Groenhof, A. R.; Ehlers, A. W.; Lammertsma, K. *J. Phys. Chem. A* **2004**, *108*, 5479.

(67) Paulsen, H.; Duelund, L.; Winkler, H.; Tolflund, H.; Trautwein, A. X. *Inorg. Chem.* **2001**, *40*, 2201.

CT100359X